JOURNAL OF MATERIALS SCIENCE 27 (1992) 6506–6512

# Elastoplastic stress analysis of a short fibre reinforced composite using a three-dimensional finite element model with several close to reality features

K. M. BROCKMÜLLER
*BASF AG Ludwigshafen Depts ZXT and ZKV/F, Ludwigshafen, Germany*
K. FRIEDRICH
*Inst. f. Composite Materials Ltd, University of Kaiserslautern, Germany*

The knowledge of stress distributions within a short fibre reinforced composite is useful for an understanding of the micromechanical load transfer between fibre and matrix. This is especially interesting in the case of a plastifying matrix about which little can be found in the literature. This paper first describes a newly developed finite element model in three dimensions which contains several closer to reality aspects than conventional models. Using this model, stress distributions are presented for an almost perfectly elastic and for a strongly plastified deformation stage of a specimen with a high degree of fibre orientation. These distributions and their implications are discussed in detail.

## 1. Introduction

The study of the stress transfer between fibres and matrix in a short fibre reinforced composite, especially for the case of non-linear material response, is a basis for further material improvement. The results obtained can be used for the improvement of analytical models and failure theories or for examining the influence of interphases between fibres and matrix. Termonia [1], Choi [2], Rainer [3], Nezbedová and Davidovič [4] and others used boundary or finite element techniques to tackle this problem. Most of these models are based on two dimensional simulations, assuming for the third dimension a plane stress, plane strain or a rotational symmetry behaviour. Other authors, for example Atkinson *et al.* [5], Phan-Thien *et al.* [6] and Di Anselmo *et al.* [7], calculated stress distributions for the matrix around a fibre placed in a large volume of matrix. All stress distributions show high concentrations at the fibre ends as well as a complicated stress transfer pattern within the matrix material.

In this paper a close to reality finite element (FE) model is described, which has the following features:

1. All fibres are aligned in the same direction. The model is therefore relevant to short fibre composites with a high degree of fibre orientation, as found for example in injection-moulded tensile test specimens [8].
2. Fibres are positioned such that the stress transfer from fibre to fibre is not merely along the fibre direction but also by shearing forces to adjacent fibres.
3. The fibres are placed in three dimensions since a real composite also has three dimensions. A reduction to two dimensions would have required an assumption on whether the model is in a plane stress, plane strain or a state of radial symmetry [2, 4].
4. Since fibres in real composites do not have a coupling agent at the ends (fibres are broken after being coated) the model assumes no contact (i.e. no load carrying capability) between fibre end and matrix.
5. The following parameters can be varied freely:

(i) Fibre length, $l_f$. This corresponds to the mean fibre length within a composite.
(ii) Fibre diameter, $d_f$.
(iii) Fibre volume fraction, $V_f$.
(iv) Elastic tensile moduli ($E_f$, $E_m$) and transverse contraction ($\nu_f$, $\nu_m$) of fibre and matrix. Plasticity of the matrix is included by input of a measured stress–strain curve of the matrix material.

This model is considered to be close to reality since a comparison of measured and calculated elastic moduli and stress strain curves shows good agreement.

The plastification of the model is approached on the basis of a von Mises criterion. The change from a perfectly elastic to a fully plastified material is documented.

## 2. Principal ideas in the development of the FE model

This new FE model was developed to push the compromise between restrictions due to available computer resources and closeness to existing composites


0022–2461 

as much as possible in the latter direction. Since a 3-D model which requires far more elements than its 2-D counterpart, seemed inevitable (see Introduction, point 3), a fibre orientation distribution could not be included. This would have required to include several fibres at different angles and relative positions to each other. This restricts the application of the model to composites with a high degree of fibre orientation.

A real composite contains fibres which are not located just behind or beside each other. Often the fibres are shifted against each other, so that there is a significant amount of shear forces between adjacent fibres. The simplest composite model (i.e. the model with the highest amount of symmetry) which takes account of these ideas is shown for the $x$–$z$ plane in Fig. 1. Following the $y$-direction, the same configuration of fibres is found again and again; however, each plane is shifted in the $z$-direction. This model of a composite is infinite in the $x$-, $y$- and $z$-directions and therefore (intentionally) contains no boundary effects. As explained in point 4 of the introduction, fibre ends in a composite should not carry any load to the matrix. Usually FE models do not treat fibre ends in this way (see, for example, References 2–4) which leads to significant stress transfer across the fibre ends.

A FE model must be finite in size. Fig. 2 shows the extraction of a unit cell from the infinite model. A repetition of this unit cell (including inversions of it) builds up completely the former model. Therefore no information is lost.

The symmetry which was used in the reduction to the unit cell establishes restrictions to the displacement modes of all nodes at the surfaces of the reduced model. These boundary conditions are also documented in Fig. 2: whenever a surface coincides with a plane of symmetry of the full model all nodes on this surface must always move by the same amount in the direction perpendicular to that surface. In the special cases of the areas with $z = z_{min} = 0$, $y = y_{min} = 0$ and $x = y$, the nodes were defined not to move away from the symmetry boundary at all. This is no *ad hoc* choice but merely the use of symmetry and the requirement of the structure being statically determinate. The load is applied by moving the nodes on the plane with $z = z_{max}$ by a distance $d$ in the $z$-direction.

The plane with $x = x_{max}$ is not an ordinary symmetry plane since the mirror image of the side $x > x_{max}$ does not coincide with the side $x < x_{max}$. However, there is a point symmetry for each node having $z = (z_{max} + z_{min})/2$. If one regards any of these nodes the following symmetry relations must hold for all nodes with the same value of $x$ and $y$:

$$U_x(\mathrm{I}) + U_x(\mathrm{J}) = 2U_x(\mathrm{K})$$
$$U_y(\mathrm{I}) + U_y(\mathrm{J}) = 2U_y(\mathrm{K})$$
$$U_z(\mathrm{I}) + U_z(\mathrm{J}) = 2U_z(\mathrm{K})$$

K is node with $z = (z_{max} + z_{min})/2$. The nodes I and J have the same $x$- and $y$-values as K, but lie symmetrical to K (one above and the other below). The terms $U_x(\mathrm{K})$, $U_y(\mathrm{K})$ and $U_z(\mathrm{K})$ take care of a general movement of the plane, which may for example be caused by Poisson contraction. The nodes I and J always move anti-symmetrically with respect to K. Without these less obvious conditions of symmetry, a model twice as large would have been necessary.

Apart from these constraints the symmetry used introduces as a free parameter the quotient $a/b$ (see Fig. 1). If everything else is kept fixed, this parameter controls how close the fibres lie together in the $x$- (respectively $y$-) and the $z$-directions. Its choice is not

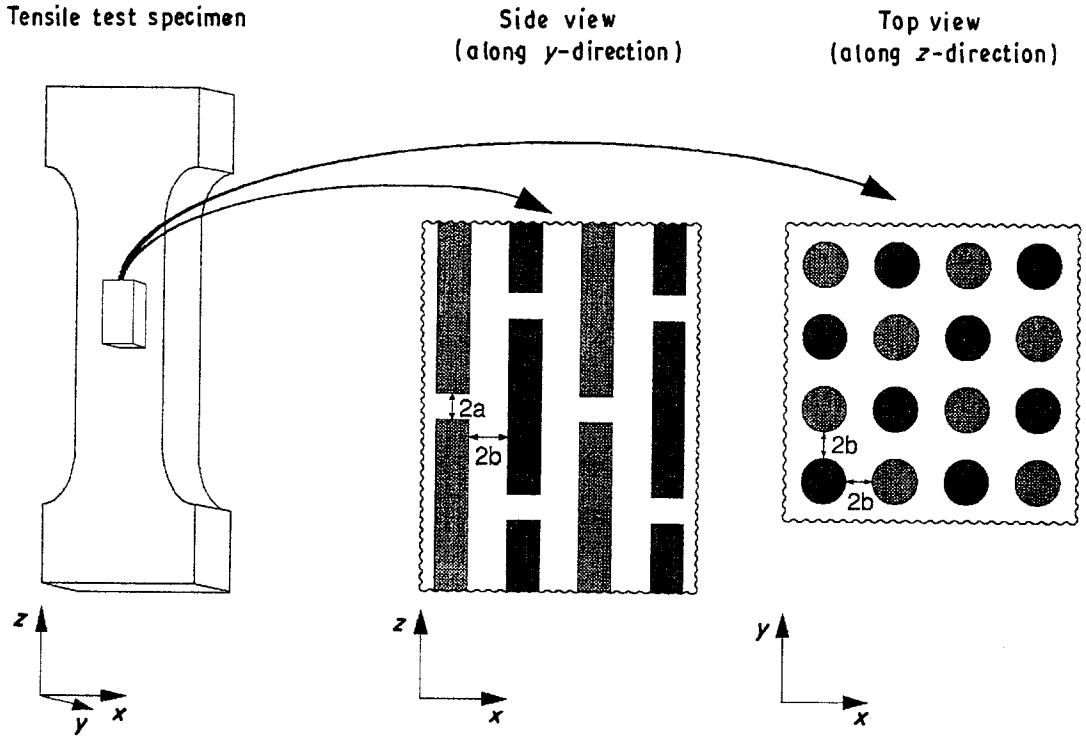


*Figure 1* Assumed relative placement of fibres within a specimen with a high degree of fibre orientation.

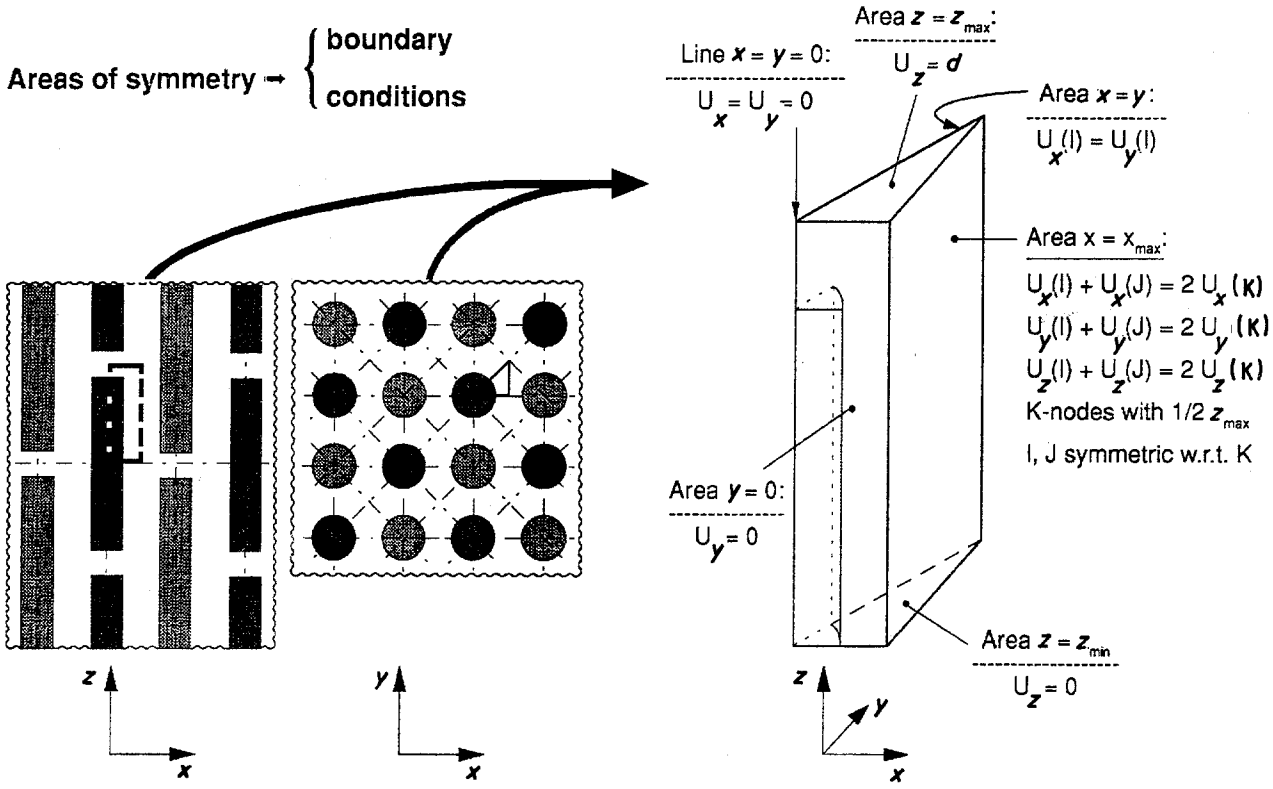


*Figure 2* Extraction of a unit cell from the infinite model of the composite.

critical as will be shown later. A good assumption for its default value seemed to be $a/b = 1$.

## 3. Details of the finite element model

The constraints at the plane with $x = x_{max}$ required a symmetrical placement of nodes with respect to those having $z = (z_{max} + z_{min})/2$. This led to the FE mesh shown in Fig. 3. The mesh is not specifically refined about the fibre end where, due to the missing connection between fibre end matrix, there is a stress singularity. This is no problem as long as high quality results in this particular region are not required. The element type used was an 8-node solid having a $2 \times 2 \times 2$ lattice of integration points with Gauss integration (ANSYS program: STIF45; ABAQUS program: C3D8).

It should be noted that, since the ANSYS program removes one translational degree of freedom of the model for each constraint equation and one for each boundary condition, it was a problem to include all constraints. This was solved by introducing nodes coupled to the "critical" nodes by very stiff springs such that a boundary condition could remove, say, the $z$-degree of freedom from a node and the displacement condition could remove it from the coupled node.

In the case of the linear elastic calculations full linearity was required from the program (i.e. all nonlinearities were turned off) so that the resulting model stiffness did not depend on the actually imposed displacement $d$.

In the case of a plastic material for the matrix, the large deflection and distortion options were turned on. The matrix plasticity was put into the model as a curve of true stress $\sigma$ versus plastic strain $\varepsilon_{pl}$(where $\varepsilon_{pl} = \varepsilon_{tot} - \varepsilon_{el} = \varepsilon_{tot} - \sigma/E_{matrix}$) as measured with a

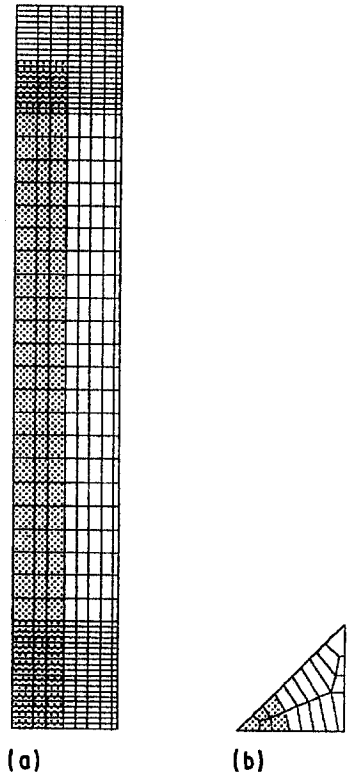


*Figure 3* Typical finite element mesh used for the calculations. This mesh was used for specimen PA6-GF-18 (see Table I); (a) $x$–$z$-plane ($y = 0$); (b) $x$–$y$-plane ($z = 0$).

tensile test specimen. This, however, merely determines the uniaxial behaviour of a material. It is not obvious, and also strongly material-dependent, how the measured behaviour can be generalized for the application of a 3-D stress state [9, 11, 12]. For the calculations the von Mises stress–strain behaviour

was assumed

$$\sigma_{vM} = [\sigma_x^2 + \sigma_y^2 + \sigma_z^2 - (\sigma_x\sigma_y + \sigma_y\sigma_z + \sigma_x\sigma_z) + 3(\tau_{xy}^2 + \tau_{yz}^2 + \tau_{zx}^2)]^{1/2} \quad (1)$$

where $\sigma_{vM}$ is the von Mises stress and $\tau$ is the shear stress. This criterion assumes that the yield of the material is independent of the equivalent pressure stress. The use of this law is not very suitable for polymers. However, finding a better law requires a better experimental foundation for 3-D stress–strain states in polymers [9].

## 4. Results

All results from elastic analyses were obtained with the ANSYS program. Results of plastic analyses were calculated with ABAQUS.

### 4.1. Elastic tensile moduli and stress–strain behaviour

For a given strain of the specimen the corresponding stress had to be determined. This was done by summing nodal forces, $F$, as follows:

$$\sigma(\varepsilon) = \frac{|\Sigma_{\text{nodes with } z=z_{max}} F_{z,i}| + |\Sigma_{\text{nodes with } z=0} F_{z,i}|}{2A} \quad (2)$$

$A$ is the cross-sectional area of the model. Note that the sum of the forces at the top and bottom of the model are not equal. This is because there is a shear transfer of forces to adjacent fibres.

This method for calculating stress was compared for the elastic case with a more straightforward method in which the stress is determined from the stored potential energy within the model

$$E_{pot} = \int_0^d F(s)ds \equiv \frac{1}{2}V\sigma\varepsilon \quad (3)$$

$E_{pot}$ is the stored energy (and is directly output by ANSYS) and $V$ is the volume of the model. The results for $\sigma$ as determined by Equation 3 are identical with those from Equation 2. Thus the use of Equation 2, which is the direct evaluation method for plastic materials, was confirmed.

Table 1 shows, for two types of GF-PA6 tensile test specimens, experimental and calculated values for the elastic tensile modulus. The data correlate very well with each other. As mentioned in the Introduction, the fibres in the test specimens are highly oriented. Also shown is the effect of a variation of the ratio $a/b$. Although a wide span of $a/b$ was covered, deviations from the default value $a/b = 1$ are in the region of 10%.

Fig. 4 shows experimental stress–strain curves for PA6 and the two types of composite specimens. In addition, the calculated curves for the latter materials are given. The measured stress–strain relation for the neat polyamide was the basis for the plasticity calculation of the matrix. As in the experiment, the calculated relations show higher stresses for the specimen having the higher fibre volume fraction. However, the calculated stresses for a given strain are much lower than in the experiment. This is probably due to the von Mises criterion used, which is not experimentally confirmed for polymers. There may also be some discrepancy due to rate-dependent creep of the material which was not included in the calculations. Of course, the assumptions made in the derivation of the model also influence the quality of the results.

TABLE I Characteristic data of two E-glass fibre (GF) reinforced polyamide 6 (PA6) specimens (e.g. PA6-GF-18 contains about 18 vol.% GF in a PA6-matrix) and calculated and experimentally obtained stiffnesses.

| Characteristic | PA6-GF-18 | PA6-GF-14 |
|---|---|---|
| Fibre radius $r_f$ (mm) | 0.007 | 0.005 |
| Fibre length, $l_f$ (mm) | 0.18 | 0.14 |
| Fibre volume fraction, $V_f$ (%) | 17.58 | 15.35 |
| Elastic tensile modulus of fibre $E_f$ (N mm$^{-2}$) | 70000 | 70000 |
| Transverse contraction ratio of fibre, $\nu_f$ | 0.35 | 0.35 |
| Elastic tensile modulus of matrix, $E_m$ (N mm$^{-2}$) | 1990 | 1990 |
| Transverse contraction ratio of matrix, $\nu_m$ | 0.42 | 0.42 |
| Experimental stiffness (N mm$^{-2}$) | 9140 | 8210 |
| 3D FE-model calculated stiffness (N mm$^{-2}$) | | |
| $a/b = 0.2$ | 10247 | 9336 |
| $a/b = 1$ | 9227 | 8491 |
| $a/b = 6$ | 9162 | 8317 |

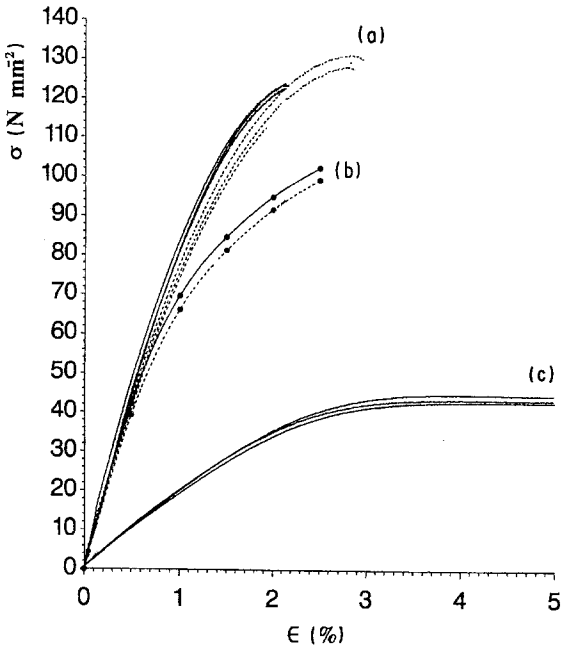


*Figure 4* Experimental and calculated stress–strain curves. Curves (a), experimental values for (——), PA6-GF-18 ($V_f$ = 17.58%) and (– – – –), PA6-GF-14 ($V_f$ = 15.35%). Curves (b), calculated values using the FE model for (–●–●–), PA6-GF-18 and (– – ● – – ● – –), PA6-GF-14. Curves (c), experimental values for PA6.

## 4.2. Stress distributions in the plasticizing model

This section and the following refer to a model made according to the specifications of specimen PA6-GF-18 as characterized in Table 1.

Figs 5–7 show the shear stress $\tau_{xz}$, the longitudinal stress $\sigma_z$ and von Mises stress $\sigma_{vM}$ for the plane with $y = 0$, respectively, as calculated for two different strain levels. At $\varepsilon = 0.5\%$ the model has an almost perfectly elastic response; at $\varepsilon = 2\%$, however, much of the matrix is plasticized. It should be noted that the displayed stresses are (deliberately) not averaged across the boundary between fibre and matrix.

The von Mises stress plot (Fig. 7) demonstrates that plastification moves from the fibre end into the matrix and then travels along the fibre towards its centre. The shear stress distribution (Fig. 5) shows that almost all the load from the fibre is transferred to the matrix by shear stresses. These are largest in the matrix region at the fibre end. Many of the shear stresses are transferred to adjacent fibres. The distribution of the longitudinal stress (Fig. 6) is included for completeness. It should be noted that the matrix moves away from the fibre end to which it was deliberately not connected.

## 4.3. Stress components along a line parallel to the fibre

As in the previous section, the reference specimen was PA6-GF-18. The stresses in the matrix close to the fibre will now be examined more closely. All the following plots refer to a straight line close to and parallel to the fibre, having $x = 1.23\ r_f$, $y = 0$ and $z$ from 0 (middle of the fibre) to 0.0972 mm ( $= z_{max}$) where $r_f$ is the fibre radius.

Figs 8 and 9 show all six stress components and the von Mises stress along this line for $\varepsilon = 0.5\%$ (quasi-elastic case) and $\varepsilon = 2\%$ (strongly plastified matrix).

1. Stress component $\sigma_z$: The stress within the fibre is least at its ends ($z = 0.09$ mm) and highest at the centre of the fibre ($z = 0$). The matrix close to the fibre is forced to have roughly the same $z$-deformation as the fibre. Therefore the $\sigma_z$-stress in the matrix is higher near the middle of the fibre and falls off towards the fibre ends. However, as the fibre has transferred all stress to the matrix before its end is reached (i.e. transfer range $z = 0$–$0.09$ mm) the $z$-stress of the matrix can rise again to higher values; a maximum was calculated at $z = 0.092$ mm. After that, it falls off again due to the shear transfer of forces to adjacent fibres.
2. Shear component $\tau_{xz}$: At the centre of the fibre the shear component in the surrounding matrix is $\tau_{xz} = 0$ since the shear forces invert at this symmetry boundary. In the elastic case, a gradual build-up of shear stress towards the fibre end can be

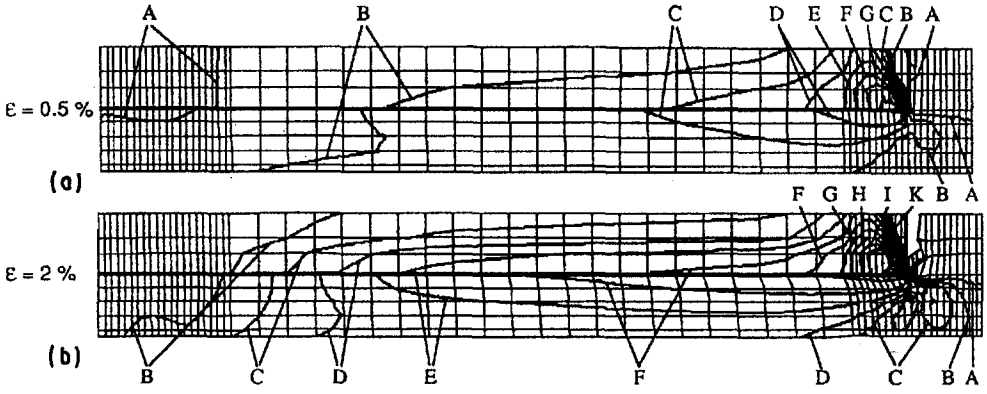


*Figure 5* Distribution of the shear stresses $\tau_{xz}$ in the plane $y = 0$ for (a) an almost perfectly elastic case ($\varepsilon = 0.5\%$) and (b) a strongly plastified model ($\varepsilon = 2\%$). The scale of the contours is as follows (N mm$^{-2}$): A = 0, B = 5, C = 10, D = 15, E = 20, F = 25, G = 30, H = 35, I = 40, J = 45, K = 50, L = 55, M = 60, N = 65, O = 70.

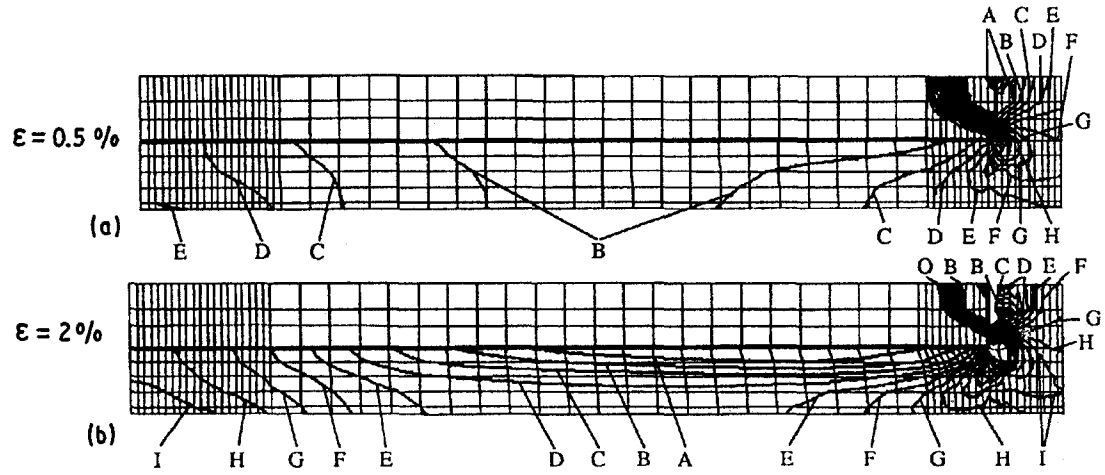


*Figure 6* Distribution of the longitudinal stresses $\sigma_z$ in the plane $y = 0$ for (a) an almost perfectly elastic case ($\varepsilon = 0.5\%$) and (b) a strongly plastified model ($\varepsilon = 2\%$). The scale of the contours is as given for Fig. 5.

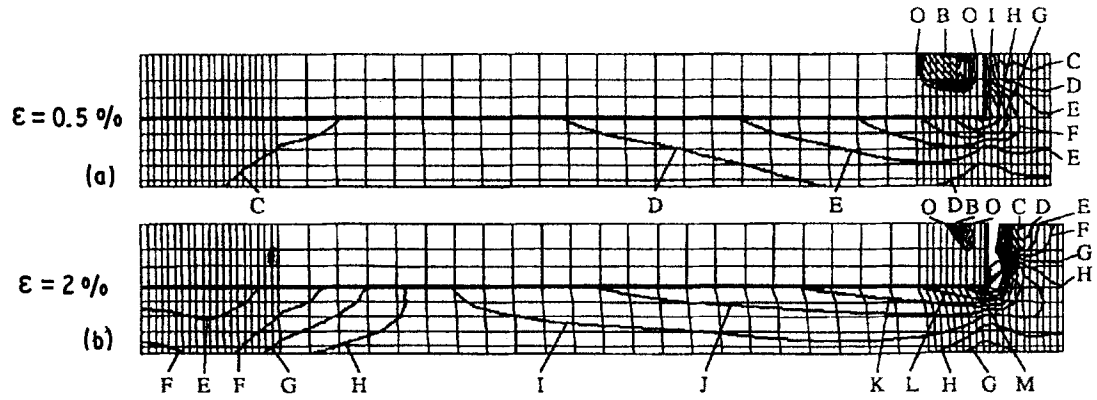


*Figure 7* Distribution of the von Mises stresses in the plane $y = 0$ for (a) an almost perfectly elastic case ($\varepsilon = 0.5\%$) and (b) a strongly plastified model ($\varepsilon = 2\%$). The load is applied to the right (positive $z$-direction).

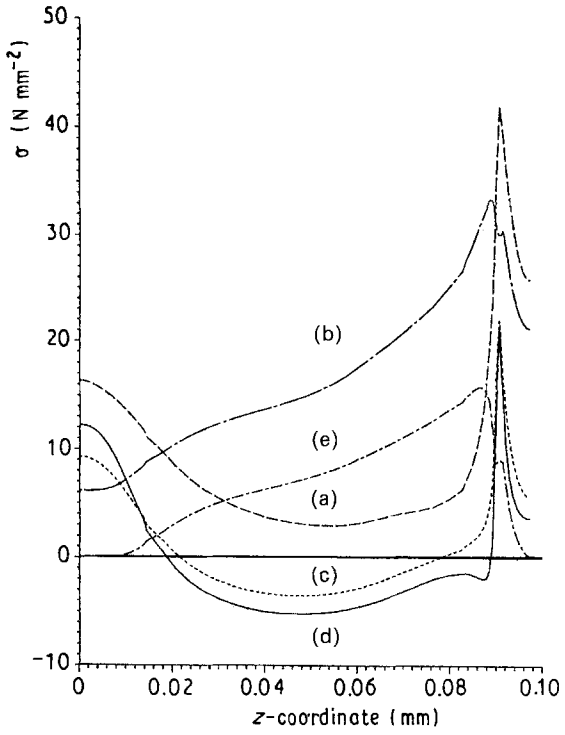


*Figure 8* Stress components within the model for a total strain of $\varepsilon = 0.5\%$. The stress field is rather complicated. The shear stress rises almost linearly with increasing $z$, in contrast with several simpler analytical theories. Curve (a), $\sigma_z$; (b) $\sigma_{vM}$; (c) $\sigma_y$; (d) $\sigma_x$; (e) $\tau_{xz}$.

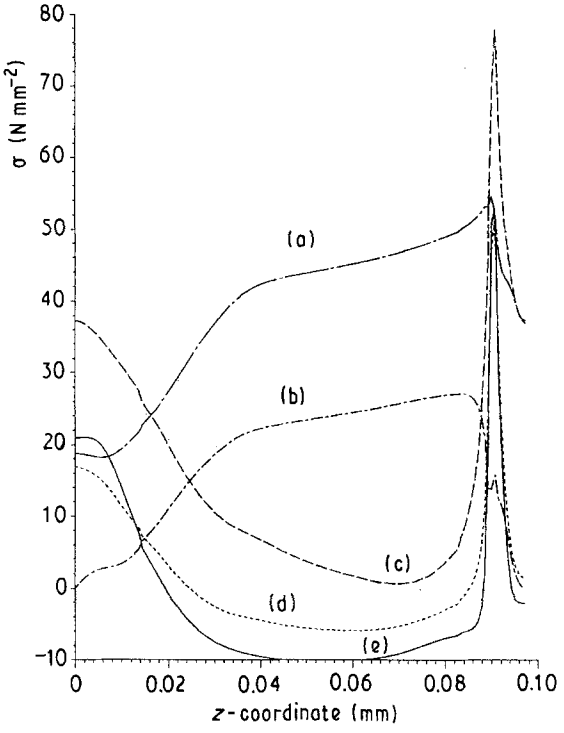


*Figure 9* Stress components within the model for a total strain of $\varepsilon = 2\%$. The von Mises stress has reached the yield stress level of the matrix (as determined in a unidirectional tensile test) over almost $\frac{1}{3}$ of the full fibre length (i.e. the matrix near the fibre is strongly plastified). Curve (a), $\sigma_{vM}$; (b) $\tau_{xz}$; (c) $\sigma_z$; (d) $\sigma_y$; (e) $\sigma_x$.

seen. In the plastic case ($\varepsilon = 2\%$, Fig. 9), this component only builds up to a value of about 25 N mm$^{-2}$. This value corresponds approximately to that which Equation 1 gives, if a yield stress of $\sigma = 43$ N mm$^{-2}$ is assumed and all other stress components (i.e. $\sigma_x$, $\sigma_y$, $\sigma_z$, $\tau_{xy}$, $\tau_{yz}$) are set to 0. This means that this shear component is the dominant stress leading to plastification.

3. Stress components $\sigma_x$ and $\sigma_y$: The matrix ahead of the top of the fibre is stressed to a certain amount in the $z$-direction. It therefore contracts. This transverse contraction causes stresses in the $y$- and $x$-directions towards adjacent fibres. This explains the elevation of $\sigma_x$ and $\sigma_y$ in the regions of the fibre ends and, due to the symmetries involved, also at the fibre centre.
4. Other stress components: The remaining shear stresses $\tau_{xy}$ and $\tau_{yz}$ are 0 for all points along the line chosen due to the symmetry of the model.

The von Mises stress distribution, $\sigma_{vM}$, shows an almost monotonic increase from a positive value in the area of the fibre centre up to a point where the matrix is fully plasticized. In this case it reaches the yield stress of the matrix (Fig. 4) and remains roughly on a constant level.

Fig. 10 shows the stress $\tau_{xz}$ along the line ($x = 1.23r_f$, $y = 0$ and $z = 0$ to $z_{max} = 0.0972$ mm) for several total deformations of the model. The narrower distances between the individual contour lines above $\varepsilon = 1.5\%$ indicate the influence of the plastification of the matrix. It also becomes evident from these results that the most endangered point for a failure of the composite is the fibre end [13, 14]. In an elastic

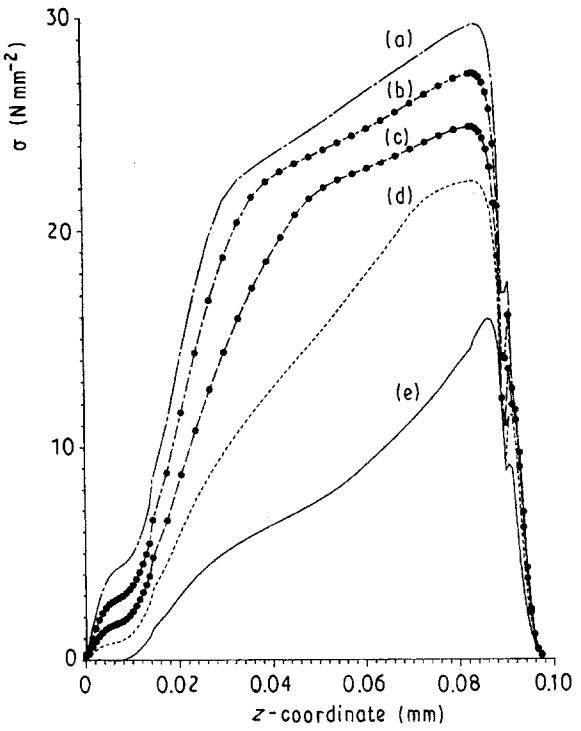


*Figure 10* Shear stress within the model for several total strains of the model. Curve (a) $\varepsilon = 2.5\%$; (b) $\varepsilon = 2\%$; (c) $\varepsilon = 1.5\%$; (d) $\varepsilon = 1\%$; (e) $\varepsilon = 0.5\%$.

calculation, there actually exists a crack tip causing a field with infinite stress at this point. In a plastic calculation the stresses are bounded by the von Mises criterion used. However, the deformation of the matrix is still largest near the fibre end.

## 5. Conclusions

A finite element model with several new and close to reality aspects was presented. The most important aspects are listed below.

(i) Fibres can transfer significant amounts of stress to adjacent fibres causing broad shear bands between adjacent fibres.

(ii) The model does not need to assume a state of plane stress, plane strain or radial symmetry since it is built up in three dimensions.

(iii) The fibre ends are not fixed to the matrix, corresponding to the fact that in reality there is no coupling agent at these places.

(iv) The model corresponds to an infinitely extended structure so that no surface effects influence the results.

(v) The physical parameters $l_f$, $d_f$, $V_f$, $E_f$, $E_m$, $\nu_f$, $\nu_m$ and a plasticity stress–strain relation can be chosen within physical bounds.

(vi) The behaviour of the model, especially for the elastic case, was shown to correspond well with experimental measurements.

(vii) The only model-inherent parameter $a/b$ was shown not to influence the model's stiffness calculation drastically.

(viii) Stress fields for a quasi-elastic state and a strongly plastified model were discussed in detail with emphasis on the effect of the relative fibre placement and the effect of the uncoupled fibre end.

(ix) The most critical region for possible failure—the matrix near the fibre end—was pointed out.

(x) The model presented here may be used for an optimization of several composite properties (for example, the elastic modulus) by variation of fibre length and radius.

An interlayer of macroscopic thickness, say 1 μm, can easily be included by a redefinition of the element material properties in the vicinity of the fibres. Such an extension of the model is under investigation at present. It may help to study how such an interphase must theoretically be optimized with regard to thickness and mechanical performance in order to achieve maximum values of energy to failure of these materials.

## Acknowledgements

K. Brockmüller is grateful for the support of BASF AG Ludwigshafen, departments ZKV/F and ZXT for financial support and valuable discussions with numerous colleagues, also from the department KTE/TM. K. Friedrich appreciates the support of the Fonds der Chemischen Industrie, Frankfurt, for his personal research activities in 1991. The topic presented here is part of a research project on the mechanical performance of discontinuous fibre reinforced thermoplastics, supported by the German Science Foundation (DFG FR 675-2-2).

## References

1. Y. TERMONIA, *J. Mater. Sci.* **22** (1987) 1733.
2. N. S. CHOI, PhD thesis, Kyushu University, Fukuoka, Japan (1990).
3. U. RAINER, *Plast. Kaut.* **5** (1983) 256.
4. E. NEZBEDOVÁ and I. DAVIDOVIČ, *ibid.* **6** (1986) 228.
5. C. ATKINSON, J. AVILA, E. BETZ and R. E. SMELSER, *J. Mech. Phys. Solids* **30** (3) (1982) 97.
6. N. PHAN-THIEN, G. PANTELIS and M. B. BUSH, *Appli. Math. Modeling* **6** (1982) 257.
7. A. DI ANSELMO, M. L. ACCORSI and A. T. DI BENEDETTO, *Compos. Sci. Technol.*, in press.
8. F. RAMSTEINER and R. THEYSOHN, *Composites* **10** (1979) 111.
9. W. SCHNEIDER and R. BARDENHEIER, *Z. Werkstofftechnik/J. Mater. Technol.* **8** (1975) 269.
10. W. SCHNEIDER and R. BARDENHEIER, *ibid.* **10** (1975) 339.
11. G. C. SIH and A. M. SKUDRA, in "Failure Mechanics of Composites", Handbook of Composites, Vol. 3, edited by G. C. Sih and A. M. Skudra (Elsevier Science, Amsterdam, 1985), p. 164.
12. L. MASCIA, "Thermoplastics: Materials Engineering", (Elsevier Science, London, 1989), p. 172.
13. N. SATO, T. KARAUCHI, S. SATO and O. KAMIGAITO, "In situ SEM observation of fracture processes in short glass fiber reinforced thermoplastic composite", Special technical publication 868, (ASTM-STP 868) (American Society for the Testing of Materials, 1985) p. 493.
14. K. FRIEDRICH, in "Application of Fracture Mechanics to Composite Materials", edited by K. Friedrich, (Elsevier Science, Amsterdam, 1989), p. 425.

*Received 28 November 1991*
*and accepted 23 January 1992*